



A novel dual mode X-band EPR resonator for rapid in situ microwave heating

Andrea Folli^{a,*}, Heungjae Choi^b, Michael Barter^b, Jaafar Harari^b, Emma Richards^a, Daniel Slocombe^b, Adrian Porch^b, Damien M. Murphy^a

^aSchool of Chemistry, Cardiff University, Park Place, Cardiff CF10 3AT, UK

^bSchool of Engineering, Cardiff University, The Parade, Cardiff CF24 3AA, UK

ARTICLE INFO

Article history:

Received 20 September 2019

Revised 4 November 2019

Accepted 8 November 2019

Available online 13 November 2019

Keywords:

Electron Paramagnetic Resonance (EPR)

T-jump

Perturbation methods

Kinetics

Resonator design

Dielectric heating

Spin probes

Copper

ABSTRACT

A unique dual mode X-band Continuous Wave (CW) EPR resonator designed for simultaneous EPR measurement and rapid microwave (MW) induced sample heating is described. Chemical reactions subjected to a flow of energy and matter can be perturbed away from the thermodynamic equilibrium by imposing a rapid shock or physical change to the system. Depending on the magnitude of the perturbation, these changes can dictate the subsequent evolution of the entire system, allowing for instance to populate non-equilibrium reactive intermediate states. Temperature jump (T-jump) experiments are a common method to achieve such perturbations. Most T-jump experiments are based on Joule Heating methods or IR lasers. Here we demonstrate the principle of rapid sample heating based on microwaves. The benefits of MW heating include (i) rapid and efficient heating (i.e. using a tuned resonant cavity, >99% efficient power transfer to the sample can be achieved), and (ii) volumetric heating (i.e. the entire sample volume rises in temperature at once, since heat is generated in the sample instead of being transferred to it). Accordingly, the key concept of the design is the use of a cavity resonator allowing EPR detection (at 9.5 GHz) and simultaneous sample heating (at 6.1 GHz). Temperature increments of 50 °C within a few seconds are possible. This is evidenced and illustrated here by probing the temperature-induced variation of the rotational dynamics of 16-doxyl stearic acid methyl ester (16-DSE) spin probe grafted on the surface of sodium dodecyl sulphate (SDS) micelles in water, as well as copper (II) acetylacetonate in chloroform. Rapid changes in the rotational dynamics of the paramagnetic centres provide direct evidence for the in situ and simultaneous EPR measurement-heating capabilities of the resonator. Improvements afforded by the use of pulsed MW sources will enable faster heating time scales to be achieved. In the longer term, this current study demonstrates the simple and direct possibilities for using MW heating as a means of performing T-jump experiments.

© 2019 The Authors. Published by Elsevier Inc. This is an open access article under the CC BY license (<http://creativecommons.org/licenses/by/4.0/>).

1. Introduction

All chemical reactions subject to a flow of energy and matter can be perturbed away from thermodynamic equilibrium by imposing a rapid shock or physical change to the system. Depending on the magnitude of the perturbation, these changes can dictate the subsequent evolution of the chemical system, revealing important information on the underlying reaction mechanism. For example, in a simple endothermic reaction in which reactant [A] converts into product [B], a rapid temperature rise will shift the equilibrium to a non-equilibrium state in which $[B]_{\text{noneq}}$ has a higher concentration compared to the equilibrium state $[B]_{\text{eq}}$.

The reaction mixture then shifts to a new equilibrium (at the new temperature) at a rate determined by the reaction kinetics. If the relaxation time from the new state reverting back to the initial equilibrium state (at the original temperature) can be monitored, then the kinetics of the reactive species can be found [1]. Alternatively, if the population of any intermediate in the reaction is increased during this process, this may then be studied spectroscopically. This is the essential basis of temperature jump (T-jump) experiments, and as a result, a considerable amount of research has been conducted over the years into new (and faster) methods of generating homogeneous T-jumps, particularly in the study of reaction kinetics or conformations (i.e. protein folding dynamics) in biophysical/biochemical [2–7] or chemical reaction systems [8].

The majority of T-jump experiments are based either on Joule Heating (requiring a conducting solution) or more commonly using

* Corresponding author.

E-mail address: folli@cardiff.ac.uk (A. Folli).

IR lasers. The latter requires a solvent or a dye with strong IR absorption properties to directly or indirectly heat the solution. Kubelka provides an excellent account on the available laser T-jump methods, particularly the many experimental considerations that must be taken into account for time resolved studies in biophysics [5]. More recently THz pulses have also been proposed as a novel means of generating ultrafast T-jump conditions [9,10]. However, an alternative approach to creating a rapid temperature rise in solution, which has been scarcely considered or utilised to date, is to use microwaves (MW) which potentially offer an incredibly effective means of heating (creating a T-jump) using a suitable resonator. Egozy and Weiss first recognised this when describing a T-jump apparatus utilising MW heating [11], although this MW approach has certainly not become mainstream in T-jump experiments to date.

From a chemical perspective, another advantage of using MW for rapid heating comes from the fact that enhancement of rates and selectivities of chemical reactions can be achieved [12], notwithstanding the many unknown origins and controversies by which MW achieve this [13,14]. In fact, the use of MW to drive chemical and catalytic reactions (also known as microwave assisted synthesis) is now well known [15–17], so that commercial MW reactors for chemical synthesis have become widely available. Reported benefits of MW in chemical reactions include shorter reaction times, higher rates, enhanced product selectivity and control of material's properties [13]. Certainly, in organic reactions, the rates can sometimes be significantly faster and in some cases the observed accelerations cannot be obtained by conventional heating methods [14]. However, in order to fully exploit the numerous benefits, there is a need to fundamentally understand how MW heating can drive and accelerate reactions.

Owing to the above two major benefits offered by MWs, for rapid heating (potentially creating T-jump capabilities) and for enhancing the rates of some chemical reactions, we sought to develop a unique dual-mode EPR resonator enabling rapid in situ heating, ultimately in order to study chemical (catalytic) reactions in solution. One mode of the resonator operates at 6.1 GHz and is used to heat the sample (in the TM_{010} mode), whilst the second mode operates at 9.5 GHz for EPR detection (TM_{110}). As mentioned above, the benefits offered by MW for rapid heating experiments are considerable. MW radiation can locally raise the temperature of the desired sample volume very rapidly, unlike conventional heated systems that are dependant on conduction and convection. Since most solvents have sufficiently high MW permittivity, very efficient volumetric MW heating can be applied to a range of systems of chemical interest. Furthermore, since quartz is a MW transparent material, the efficiency of heating will not be affected by the EPR tubes used in the proposed dual mode resonator. In this current work, we describe the basic principles of the resonator, designed for simultaneous heating and EPR experiments, and demonstrate how rapid heating can be achieved using a series of radicals and paramagnetic metal centres.

2. Experimental

2.1. Resonant cavity design

An important design consideration for the dual mode resonator is that the MW heating mode must be resonant well below the cut-off frequency of the X-band waveguide used to couple to the EPR detection mode (i.e. below 6.5 GHz, assuming a waveguide “long” dimension of 22.9 mm). To meet this condition, resonant frequencies for the heating and EPR modes in the ratio of around 1.0 to 1.6 are easily achieved by designing the dual mode resonator to be near square or cylindrical (see below for details). A short length

of waveguide feed (common to all Bruker X-band EPR instruments) then acts as an almost perfect high pass filter for our dual mode resonator, rejecting the heating frequencies around 6 GHz whilst transmitting the EPR frequencies around 9.5 GHz. For a perfectly cylindrical cavity resonator of internal radius R , the resonant frequencies of the TM_{010} and TM_{110} modes can be calculated very precisely using the following equations:

$$\begin{cases} f_{010} = \frac{p_{01}c}{2\pi R} \\ f_{110} = \frac{p_{11}c}{2\pi R} \end{cases} \quad (1)$$

where c is the speed of light in vacuo, $p_{01} = 2.405$ and $p_{11} = 3.832$ (i.e. the first roots of the Bessel functions $J_0(x)$ and $J_1(x)$, respectively). The TM_{010} and TM_{110} modes have antinodes of electric and magnetic field, respectively, on the axis and so are ideal for heating and EPR, respectively. The TM_{110} mode is doubly degenerate, with the two degenerate modes having orthogonal fields. To lift this degeneracy, so that the resonant frequencies of this mode are spectrally separated by at least 500 MHz at 10 GHz (i.e. by 5%), we chose an elliptical (rather than cylindrical) geometry. Whilst we can achieve a similar splitting of the degeneracy using a near square, rectangular cavity, the separation of the two quasi TM_{110} degenerate modes in the elliptical case is greater. There is also then a slightly better separation of the electric and magnetic fields near the cavity axis, which is important for maintaining a high quality factor (Q) for EPR measurements when lossy dielectric samples are being studied (e.g. species within any polar solvent). Whilst analytical expressions exist for the resonant frequencies of an elliptical cavity, simple, first-order approximations can be deduced from perturbations of the cylindrical cavity. For an ellipse of semi-major and semi-minor axes a and b , respectively, the resonant frequencies of the quasi TM_{010} and TM_{110} modes can be estimated using the following equations:

$$\begin{cases} f_{010} \approx \frac{p_{01}c}{\pi(a+b)} \\ f_{110,b} \approx \frac{p_{11}c}{2\pi(a-\Delta)}, f_{110,a} \approx \frac{p_{11}c}{2\pi(b+\Delta)}, \Delta = \frac{1}{2}(a-b) \end{cases} \quad (2)$$

The internal dimensions of the elliptical cavity to be used as the dual mode resonator are $a = 19.7$ mm and $b = 17.8$ mm, giving approximate resonant frequencies from Eqs. 2 of $f_{010} \approx 6.1$ GHz, $f_{110,b} \approx 9.5$ GHz and $f_{110,a} \approx 10.0$ GHz. COMSOL Multiphysics simulations of these resonant modes and their field orientations are shown in Fig. 1.

The internal length of the cavity is chosen to be 11 mm, which is large enough to ensure high unloaded Q of the TM_{010} and $TM_{110,b}$ (approximately 7000 and 8000, respectively, when the cavity resonator is constructed from aluminium), but short enough to maintain the uniformity of the modulation field and to ensure that TE modes are pushed to higher frequencies (e.g. above 14 GHz for TE_{111}). Another special feature of this cavity resonator is its construction in two parts, rather than the usual three. As can be seen from Fig. 2, all of the wall currents flow parallel to the single metal-metal join, meaning that Q is independent of the pressure applied to this contact and the resonator can be easily taken apart (separated) for occasional cleaning, whilst retaining near identical performance. Finally, it should be noted that the side walls of the cavity are very thin (around 1 mm thickness) so that the modulation field at the sample is not detrimentally compromised by the skin effect in the cavity walls.

2.2. Helmholtz coils

To obtain the required phase sensitive detection at 100 kHz, a set of Helmholtz coils were designed and constructed in order to modulate the external magnetic field B_0 . The coils were made of resistive copper wire of 0.25 mm gauge, appropriately wound so

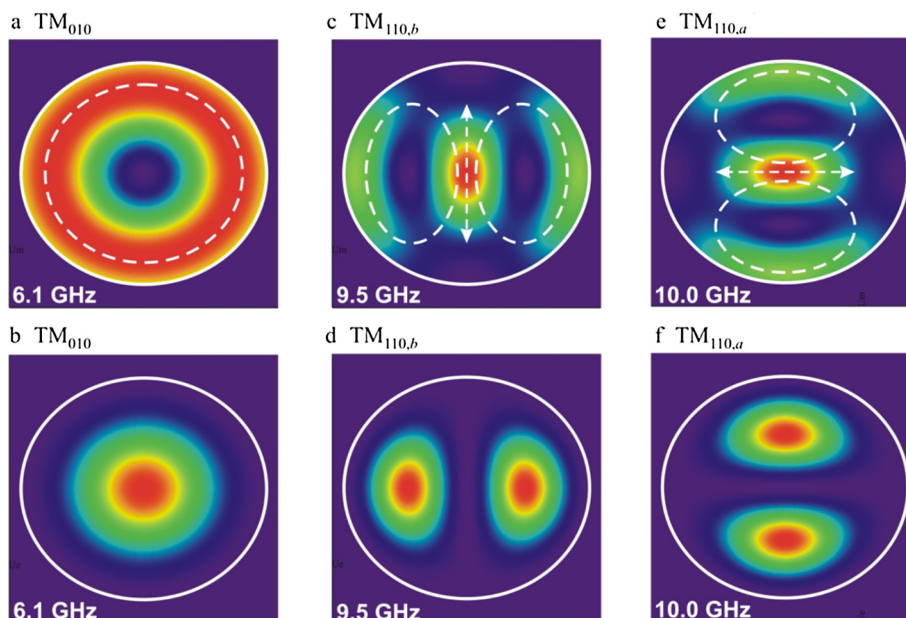


Fig. 1. Magnetic (a, c, e) and electric (b, d, f) energy densities (H^2 and E^2 , respectively) of an elliptical cavity. The approximate resonant frequencies are shown for semi-major and semi-minor axes of $a = 19.7$ mm and $b = 17.8$ mm. The H fields are in the plane of the page, whereas the E fields are perpendicular to the page.

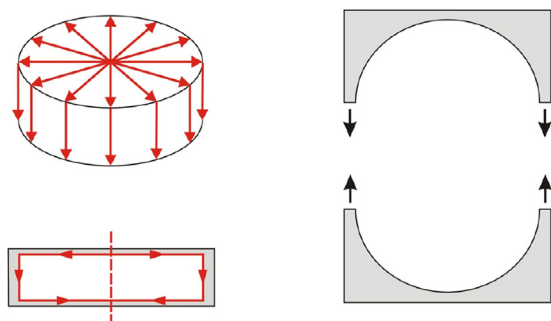


Fig. 2. Design and construction considerations of the elliptical cavity. It is manufactured in two sections to ensure that there is no current flow across metal-metal join in both the heating mode and the EPR mode (the internal surface microwave currents are shown for the TM_{010} heating mode). The metal thickness of the opposing elliptical surfaces is very thin (1 mm) to minimise the reduction in the modulation field owing to the skin depth in the cavity walls at modulation frequencies up to 100 kHz.

that the wire becomes two solenoids in series. The coils were designed to have a radius equal to the separation of the coils. The resistance and inductance of the designed Helmholtz coils were 3.482Ω and $217 \mu\text{H}$ respectively.

2.3. Experimental assembly for simultaneous microwave-assisted rapid heating and EPR measurement

The experimental assembly for the simultaneous microwave-assisted rapid heating and EPR detection is schematically illustrated in Fig. 3. The assembly consists of: a microwave signal generator (EXG 5173B, Keysight Technologies), a DC power supply (not shown in the Figure, EA PS 2042-20B, Elektro-Automatik), a power amplifier (1131-BBM5K8CGM, EMPOWER RF SYSTEMS), a circulator (Mini-circuits), attenuators (Mini-circuits), a power sensor (U2021XA, Keysight Technologies), a thermal imaging camera (TIM640, Micro-Epsilon) and a Bruker EMX EPR spectrometer, housing the dual mode resonator equipped with Helmholtz coils described in the previous section. The MW bridge employed is a

Bruker ER041X X-band Gunn diode bridge. The resonator was designed with an observation hole to one side in order to capture real-time thermal images of the sample under test during microwave heating (and later will be used for in situ irradiation experiments). The power amplifier has a saturated output power of 40 W and 10 W at 1 dB compression point, which is more than enough to induce thermal gradients greater than 50°C in a few seconds. A circulator is added to protect the power amplifier from the reflected power (which is typical for a resonator with high quality factor) and also to monitor the power delivered to the sample. For the purposes of the initial heating experiments described in this work, a thermal imaging camera was used to record the temperature. The accurate determination of temperature in solutions heated by MW is surprisingly complex [18]. More detailed EPR thermometry approaches [19,20] will therefore be employed in our ongoing studies to accurately determine the in situ temperature achieved using the MW in the dual mode resonator.

2.4. Sample preparation for EPR

To test the dual mode capabilities of the resonator for simultaneous heating and EPR measurement, two different samples were prepared; an organic spin label and a transition metal (copper) complex.

In the first case, a 1 mM solution of 16-doxyl stearic acid methyl ester (16-DSE) in ethanol was prepared by dissolving 4 ml of 16-doxyl stearic acid methyl ester in 10 ml of ethanol. The solution was left overnight to evaporate off the ethanol. A 50 mM solution of sodium dodecyl sulfate (SDS) in water was prepared by dissolving 0.1442 g of SDS in 10 ml of water. This solution was then added to the 16-DSE residue for the SDS micelles to adsorb the 16-DSE on the micelle surface. An aliquot of the spin labelled micelle solution was then introduced into a Q-band EPR tube (1.6 mm outer diameter, 1.1 mm inner diameter suprasil tube, product number: WG-222T-RB Wilmad Labglass) for measurement with the dual-mode MW-EPR resonator.

In the second experiment, a 10 mM solution of Cu(II) acetylacetonate, $\text{Cu}(\text{acac})_2$, was prepared by dissolving 7.91 mg of $\text{Cu}(\text{acac})_2$ previously recrystallised in 3 ml of chloroform. An aliquot of the

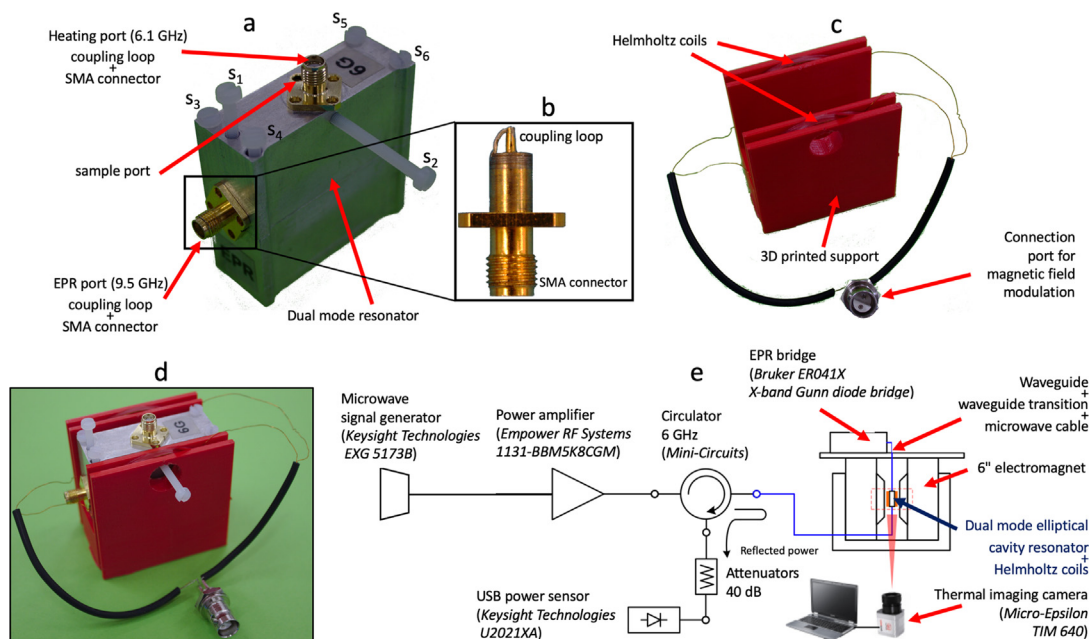


Fig. 3. (a) Details of the dual mode cavity resonator. s_1 and s_2 are two PTFE screws to hold in place the coupling loops once the two modes (TM_{010} and $TM_{110,b}$) are critically coupled. s_3 , s_4 , s_5 and s_6 are PTFE screws to hold the two parts of the resonator together. Details of the coupling loops + SMA connectors used for matching both resonant modes are shown in (b). (c) Details of the Helmholtz coils used to achieve modulation of the external magnetic field. A picture of the resonator inside the support with the Helmholtz coils is shown in (d). A schematic diagram of the experimental setup for running EPR and dielectric heating simultaneously is shown in (e).

prepared solution was introduced into an X-band EPR tube (3.0 mm outer diameter, 2.2 mm inner diameter suprasil tube, product number: 705-SQ-250 M Wilmad Labglass) for measurement with the dual mode MW-EPR resonator. EPR spectra were simulated using the Easyspin package [21] running within the Mathworks Matlab environment.

3. Results and discussion

The experimental determination of the resonance frequencies for both TM_{010} and $TM_{110,b}$ modes was achieved by critically coupling the dual mode resonator with both ports simultaneously connected to an S5180 network analyser (Copper Mountain Technologies) operating between 100 kHz and 18 GHz. The results are summarised in Table 1 for the resonator either air-filled or containing a Q-band tube filled with deionised water. We found that a compromise between the two TM modes during critical coupling was very important. Indeed, whilst we were able to achieve -50 dB on the EPR mode (i.e. $TM_{110,b}$), this limits the reflection coefficient of the heating mode (i.e. TM_{010}) to below -15 dB. In contrast, by limiting the EPR mode to around -30 dB, this allows us to maintain -15 dB to -30 dB for the heating mode (see Table 1), which is preferable for power delivery to achieve the desired temperature increases.

Using the network analyser with both ports connected, we were also able to obtain values for the Q factor. This was first monitored with a weakly coupled resonator so that the measured Q could be

considered *unloaded*. The measured Q factors were 6007 for the TM_{010} mode and 7349 for the $TM_{110,b}$ mode.

The efficiency of the MW induced heating was shown using an IR thermal imaging probe and 50 μ l of water in a Q-band EPR tube when setting the MW source to deliver a nominal power of 1 W at 6.1 GHz. Fig. 4 shows the temperature ramp achieved. The initial slope of the curve indicates a temperature ramp of $1.57 \text{ K}\cdot\text{s}^{-1}$. Power losses in the cables connecting the MW source to the amplifier and subsequently the amplifier to the resonator, plus the power loss within the resonator itself (associated with the Q-factor at 6.1 GHz) would decrease the actual power available to heat the sample. In simple terms, considering that the specific heat capacity of water is equal to $4.18 \text{ kJ}\cdot\text{kg}^{-1}$ and assuming $>99\%$ absorbance of the MW radiation, it can be deduced that 1 W of nominal power would cause a temperature rise of $4.78 \text{ K}\cdot\text{s}^{-1}$ on 50 μ l of water, if no power was lost. Hence, we can estimate that the power transfer efficiency in the entire system is $1.57 \text{ K}\cdot\text{s}^{-1} / 4.78 \text{ K}\cdot\text{s}^{-1} = 0.33$. Even with this low power transfer efficiency, it can be calculated that when using 10 μ l of water rather than 50 μ l (i.e. which is the case for many solution samples analysed by EPR spectroscopy in Q-band tubes), a T-jump of 5 K in just over 20 μ s would require a MW power of 30 W at 6.1 GHz, which is already possible with our hardware (currently the maximum power deliverable is ca. 31 W). In addition, further hardware developments are being undertaken to improve the power transfer efficiency of the system and potentially deliver even faster T-jumps. Within the current development plan, an important issue

Table 1
Resonant frequencies and voltage standing wave (VSW) reflection coefficients for the matched cavity with and without sample.

Sample	TM_{010} mode		$TM_{110,b}$ mode	
	Resonance Frequency GHz	Reflection coefficient dB	Resonance Frequency GHz	Reflection coefficient dB
Air-filled cavity	6.180938	-32	9.587420	-31
Deionised water	6.124125	-15	9.585420	-28

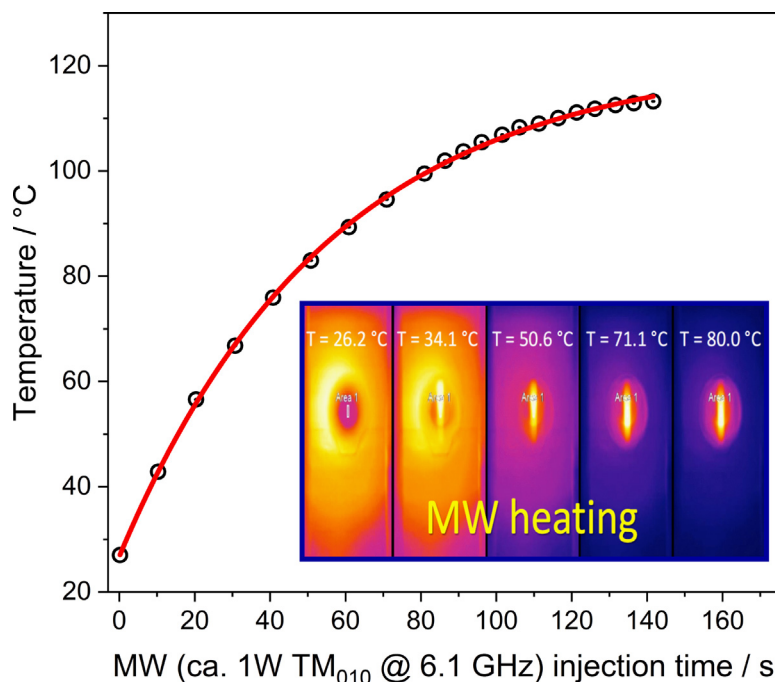


Fig. 4. Typical temperature ramp profile achievable upon continuous wave MW injection of 1 W of nominal power at 6.1 GHz. The inset is a collection of five thermo-camera images showing a water-filled EPR tube inside the cavity being subjected to dielectric heating.

that is being tackled is the control of the temperature following fast T-jump events, which at the moment is still not optimised.

After interfacing the dual mode resonator to the Bruker bridge, the modulation coils and the spectrometer signal channel were calibrated at 100 kHz modulation frequency using a BDPA (3-bisdiphenylene-2-phenylallyl) X-band EPR standard. This procedure ensured ease of operation by enabling the dual mode resonator to be controlled through the Bruker WinEPR software. After calibration, the EPR spectrum of the BDPA standard was analysed for correct spectrometer response in terms of field modulation amplitude at 0.1 mT, and modulation phases at 0°, 90° and 180°. The results of the test demonstrating resonator and system performance are shown in Fig. 5.

Fig. 5(a)-(d) shows that in terms of modulation phase, the calibration routine was successful, as demonstrated by the complete loss of signal at 90° modulation phase and full reversibility at 180° modulation phase. Nevertheless, the line width of the BDPA resonance line is narrower than expected. The intrinsic line width of the BDPA radical is narrower than 0.1 mT, therefore at 100 kHz field modulation frequency and 0.1 mT field modulation amplitude, one would expect the resonance line to be over-modulated, hence approximately equal to 0.1 mT (i.e. the modulation depth). The fact that the Lorentzian fitting returned ca. 60% of the expected value matches results obtained with a set of search coils positioned inside the resonator which highlighted that only 60% of the modulation field generated by the Helmholtz coils actually enters the cavity.

The first proof-of-concept of dielectric heating was performed using SDS micelles in water, spin-labelled with 16-DSE. Fig. 6(a) shows the X-band CW EPR spectrum of the spin-labelled micelle at room temperature. The spectrum can be fitted to a model of anisotropic rotational diffusion, with a rotational diffusion tensor exhibiting axial symmetry, i.e. with a preferential rotation mode, and identified by the diagonalised matrix in Eq. (3):

$$\mathbf{D}_r = 10^8 \begin{bmatrix} 5.208 & 0 & 0 \\ 0 & 4.505 & 0 \\ 0 & 0 & 4.505 \end{bmatrix} \frac{1}{s} \quad (3)$$

Following 20 s of 1.5 W (nominal power) MW injection at 6.14 GHz, which causes the temperature of the sample to rise to about 58 °C, the EPR spectrum changed to that shown in Fig. 6 (b). This second spectrum can still be simulated and fitted to a model of anisotropic rotational diffusion, but at a much faster rate compared to the original room temperature case, as evidenced by the new rotational diffusion tensor in Eq. (4).

$$\mathbf{D}_r = 10^{10} \begin{bmatrix} 1.834 & 0 & 0 \\ 0 & 0.1834 & 0 \\ 0 & 0 & 0.1834 \end{bmatrix} \frac{1}{s} \quad (4)$$

Interestingly, the rotational diffusion not only increases at higher temperature, but also becomes more anisotropic. Faster rotational diffusion rates are expected at higher temperature, given the reduced viscosity of the solvent. For example, the viscosity of water decreases from 1.00 mPa·s (or cP) at 20 °C (0.90 mPa·s at 25 °C) to just below 0.50 mPa·s at ca. 58 °C [22]. It should be noted however, that in addition to changes in solvent viscosity, the supramolecular aggregation of SDS surfactant molecules is also temperature dependent. At the concentration of SDS surfactant used in this study, the SDS micelle ellipsoid volume is expected to change from ca. $2.8 \cdot 10^4 \text{Å}^3$ to $1.8 \cdot 10^4 \text{Å}^3$ [23], greatly induced by the change of the micelle aggregation number (i.e. average number of surfactant molecules per micelle) from ca. 65 (at RT) to ca. 35 (at 58 °C) [23]. Whilst changes in viscosity would be expected to reflect isotropically on the rotational diffusion, a different physical-chemical interaction of the spin label with a smaller micelle (on average) seems to allow for an even increased preferred rotation of one of the possible modes over the other two.

The second experiment to test the performance of the resonator was conducted using a solution of copper (II) acetylacetonate, Cu

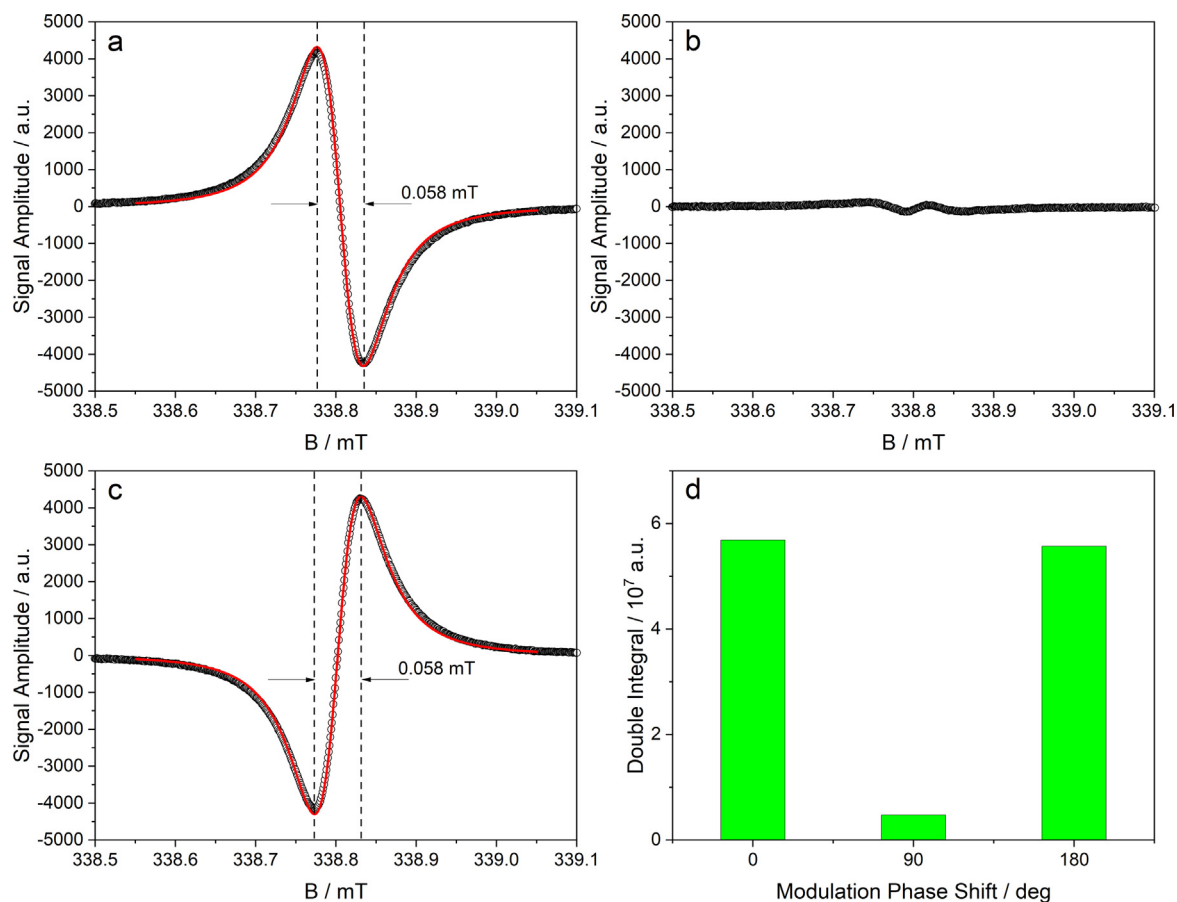


Fig. 5. X-band CW EPR spectra of the BDPA standard following calibration of the Bruker EMX signal channel with the dual mode cavity resonator and Helmholtz coils. Black empty circles indicate the experimental points whilst the red solid lines are the fitting to a pure Lorentzian line shape (first harmonic). Spectra were recorded at 100 kHz field modulation frequency, 0.1 mT field modulation amplitude and (a) 0°, (b) 90°, (c) 180 °C modulation phase. Receiver gain (10^4), time constant (5.12 ms), conversion time (10.24 ms), and number of points (4096) were kept constant for all the spectra. (d) Calculated double integrals of the BDPA spectra in (a), (b) and (c). (For interpretation of the references to colour in this figure legend, the reader is referred to the web version of this article.)

($C_5H_7O_2$)₂, dissolved in $CHCl_3$ as a paradigmatic system. This was chosen as a simple standard to represent a transition metal complex. Fig. 7(a) shows the X-band CW EPR spectrum of the complex at room temperature. The spectrum was simulated and fitted to a model of isotropic rotational diffusion, with an isotropic rotational correlation time of ca. 20 ps. Upon dielectric heating at 56 °C, the EPR spectrum changed to that shown in Fig. 7(b), which is fully consistent with the spectrum reported by Wilson and Kivelson [24] for the same compound in the same solvent at 58 °C using conventional heating. Fitting the high temperature spectrum to the same model used for the RT spectrum revealed a new isotropic rotational correlation time of ca. 11 ps, in line with a faster rotational diffusion which is mostly caused by a decreased solvent viscosity as driven by the MW induced increase in temperature. Upon comparison of the spectrum in Fig. 7(a) with the one in Fig. 7(b), it is also possible to identify a slight decrease of the signal-to-noise ratio. We discovered that the power amplifier for the 6.1 GHz microwave source generates higher harmonics at ca. 12 GHz. These propagate unfiltered into the EPR microwave bridge, leading to partial detuning of the 9.5 GHz mode employed for EPR detection. This is also confirmed by the double integrals of the spectra during heating. Over three consecutive heating/cooling cycles, the spectra recorded during MW injection at 6.1 GHz (Fig. 7(c)) exhibited systematic smaller values (i.e. partial loss of signal) when compared to the spectra without MW injection at 6.1 GHz. Further technological developments are currently being undertaken to filter out these higher harmonics before they reach the EPR microwave bridge.

4. Perspective for T-jump EPR experiments

Microwaves can be used to accelerate and drive chemical reactions in a very efficient manner. If the MW field is applied to the sample in a resonant mode, such that the E-field component of the radiation is selected, then incredibly efficient heating can be achieved. Although the precise mechanism by which the MW can heat liquids and solids is not comprehensively understood, this has not deterred the wide spread use of MW reactors in chemical synthesis. Rapid heating can change not only the selectivity of some reactions, but also provides a simple and effective means to study the kinetics and dynamics of the reacting system itself via the temperature-jump relaxation approach. Most chemical reactions involve an equilibrium process, with the rate of the forward and reverse reactions controlling the overall concentration of reactants and products at any given point in time. The chemical or conformational equilibrium can be easily perturbed and shifted in either direction, when a stress is applied. This stress may involve a change in concentration, pressure or temperature. The rate of change from the old to the new equilibrium will depend on the rate constant for the forward and reverse reactions or the conformational change, so that analysis of this rate is extremely informative in chemical kinetics and dynamics. It is important that the perturbation is applied more rapidly than the relaxation time, and usually on a time scale that is faster than the mixing times involved. Rapid heating by microwaves (creating a T-jump) using a suitable resonator, could therefore be used as a novel means of studying

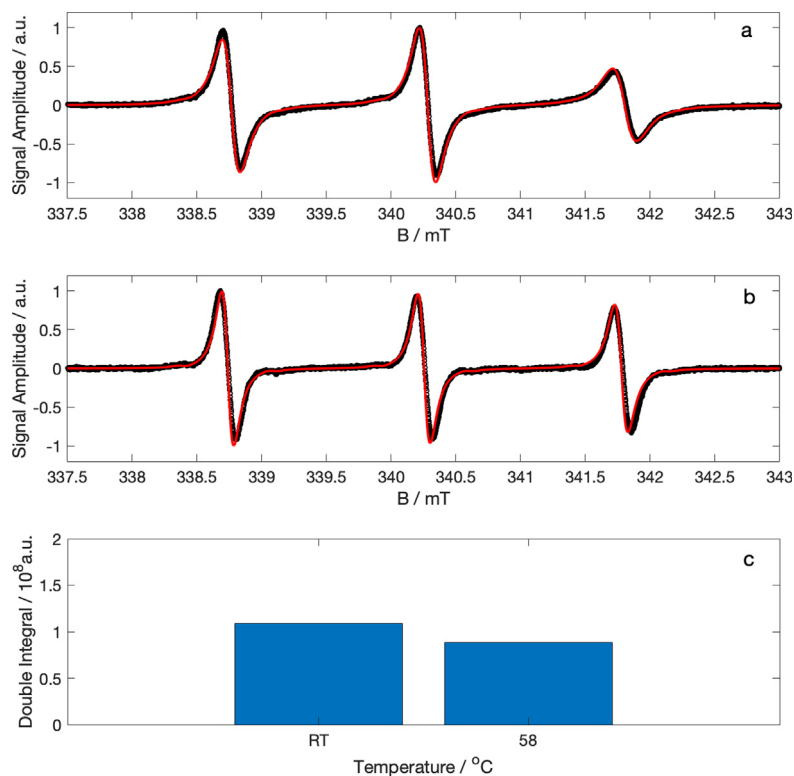


Fig. 6. X-band CW-EPR spectra of 16-DSE spin-labelled SDS micelles in water recorded at (a) room temperature, and (b) 58 °C. Spectra were recorded using the dual mode resonator operating at 100 kHz field modulation frequency, 0.1 mT field modulation amplitude, $5.024 \cdot 10^{-4}$ receiver gain and 4096 points. (c) Double integrals of the spectra in (a) and (b).

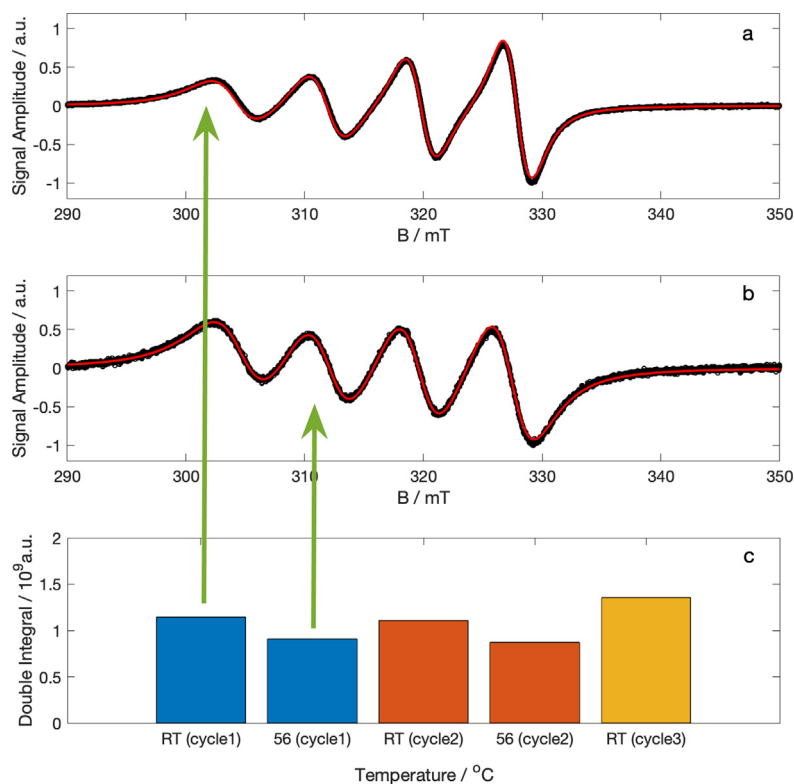


Fig. 7. X-band CW-EPR spectra of $\text{Cu}(\text{C}_5\text{H}_7\text{O}_2)_2$ in CHCl_3 recorded at (a) room temperature, and (b) 56 °C. Spectra were recorded using the dual mode resonator operating at 100 kHz field modulation frequency, 0.1 mT field modulation amplitude, $3.991 \cdot 10^{-4}$ receiver gain and 4096 points. (c) Double integrals of the spectra in (a) and (b), plus double integrals of spectra recorded during three further heating/cooling cycles whose EPR spectra are not shown.

reaction kinetics and dynamics, as well as investigating the fundamental mechanism of how MW influence chemical reactions. The greatest advantage offered by MW heating is the near homogeneous, controlled, volumetric heating state that can be almost instantaneously achieved, particularly using short MW pulses.

In the current work, the MW field was delivered to the sample under continuous irradiation conditions using the 6.1 GHz heating mode in the resonator. Successful in situ heating was evidenced by the changes in rotational correlation time (monitored simultaneously by EPR) for two different paramagnetic systems. The use of pulsed MW sources at 6.1 GHz will enable us to deliver faster temperature rises in a controlled fashion, to study by EPR spectroscopy dynamics and kinetics in chemical systems. Crucially, this resonator is simple to produce and easy to use on a standard Bruker EPR spectrometer, offering a facile method for in situ EPR heating studies.

5. Conclusions

In this paper, we have described a novel dual-mode EPR resonator capable of performing standard X-band EPR measurements whilst simultaneously enabling the in situ dielectric volumetric heating of the sample using microwaves. We have demonstrated the successful EPR detection of a spin-labelled system and a transition metal (copper) complex under dielectric heating conditions, as evidenced by the changes in the rotational diffusion dynamics of the paramagnetic species in solution. Providing the availability of a suitable microwave generator at 6.1 GHz and a suitable amplifier, this resonator can be easily interfaced to a Bruker EPR microwave bridge and operated using the standard Bruker instrumental software. The currently available method allows for modest T-jumps of over 50 °C in a few seconds. However, further developments are underway to generate very short and high power MW pulses capable of delivering much shorter T-jumps within a few μ s or faster. We envisage a great interest from scientists and researchers involved in the study of the kinetics of paramagnetic intermediate and excited states relevant to catalysis, as well as the possibility to couple this technology with high pressure EPR cells in order to monitor the kinetic evolution of paramagnetic species and intermediates over a (T,P) landscape.

Declaration of Competing Interest

The authors declare that they have no known competing financial interests or personal relationships that could have appeared to influence the work reported in this paper.

Acknowledgement

EPSRC funding (EP/R04483X) is gratefully acknowledged. Information on the data underpinning the results presented here, including how to access them, can be found in the Cardiff University data catalogue at <http://doi.org/10.17035/d.2019.0088702672>.

Appendix A. Supplementary material

Supplementary data associated with this article can be found, in the online version, at <https://doi.org/10.1016/j.jmr.2019.106644>.

References

- [1] K.A. Connors, *Chemical kinetics: The Study of Reaction Rates in Solution*, Wiley-VCH, 1998.
- [2] R. Callender, R. Dyer, Probing protein dynamics using temperature jump relaxation spectroscopy, *Curr. Opin. Struct. Biol.* 12 (5) (2002) 628–633, [https://doi.org/10.1016/S0959-440X\(02\)00370-6](https://doi.org/10.1016/S0959-440X(02)00370-6), URL <<http://www.sciencedirect.com/science/article/pii/S0959440X02003706?via%3Dihub>>.
- [3] W.A. Eaton, V. Muñoz, S.J. Hagen, G.S. Jas, L.J. Lapidus, E.R. Henry, J. Hofrichter, Fast Kinetics and Mechanisms in Protein Folding, *Ann. Rev. Biophys. Biomolec. Struct.* 29 (1) (2000) 327–359, <https://doi.org/10.1146/annurev.biophys.29.1.327>, URL <<http://www.annualreviews.org/doi/10.1146/annurev.biophys.29.1.327>>.
- [4] M. Gruebele, J. Sabelko, R. Ballew, J. Ervin, Laser Temperature Jump Induced Protein Refolding, *Acc. Chem. Res.* 31 (1998) 699–707, <https://doi.org/10.1021/AR970083X>, URL <<https://pubs.acs.org/doi/abs/10.1021/ar970083x>>.
- [5] J. Kubelka, Time-resolved methods in biophysics. 9. Laser temperature-jump methods for investigating biomolecular dynamics, *Photochem. Photobiol. Sci.* 8 (4) (2009) 499, <https://doi.org/10.1039/b819929a>, URL <<http://xlink.rsc.org/?DOI=b819929a>>.
- [6] R. Narayanan, L. Zhu, Y. Velmurugu, J. Roca, S.V. Kuznetsov, G. Pehna, L.J. Lapidus, A. Ansari, Exploring the energy landscape of nucleic acid hairpins using laser temperature-jump and microfluidic mixing, *J. Am. Chem. Soc.* 134 (46) (2012) 18952–18963, <https://doi.org/10.1021/ja301218e>, URL <<http://pubs.acs.org/doi/10.1021/ja301218e>>.
- [7] R.S. Phillips, E.W. Miles, P. Mcphie, S. Marchal, C. Georges, Y. Dupont, R. Lange, Pressure and temperature jump relaxation kinetics of the conformational change in salmonella typhimurium tryptophan synthase L -serine complex: large activation compressibility and heat capacity changes demonstrate the contribution of solvation, *J. Am. Chem. Soc.* 130 (2008) 13580–13588.
- [8] H. Ma, C. Wan, A.H. Zewail, Dynamics of ligand substitution in labile cobalt complexes resolved by ultrafast T-jump, *Proc. Natl. Acad. Sci.* 105 (35) (2008) 12754–12757, <https://doi.org/10.1073/pnas.0806869105>, URL <<http://www.ncbi.nlm.nih.gov/pubmed/18725628>>. <<http://www.pubmedcentral.nih.gov/articlerender.fcgi?artid=PMC2522261>>.
- [9] P.K. Mishra, V. Bettaque, O. Vendrell, R. Santra, R. Welsch, Prospects of using high-intensity THz pulses to induce ultrafast temperature-jumps in liquid water, *J. Phys. Chem. A* 122 (23) (2018) 5211–5222, <https://doi.org/10.1021/acs.jpca.8b00828>, URL <<http://pubs.acs.org/doi/10.1021/acs.jpca.8b00828>>.
- [10] S.L. Veber, S.V. Tumanov, E.Y. Fursova, O.A. Shevchenko, Y.V. Getmanov, M.A. Scheglov, V.V. Kubarev, D.A. Shevchenko, I.I. Gorbachev, T.V. Salikova, G.N. Kulipanov, V.I. Ovcharenko, M.V. Fedin, X-band EPR setup with THz light excitation of Novosibirsk Free Electron Laser: Goals, means, useful extras, *J. Magn. Reson.* 288 (2018) 11–22, <https://doi.org/10.1016/j.jmr.2018.01.009>, URL <<https://www.sciencedirect.com/science/article/pii/S1090780718300211?via%3Dihub>>.
- [11] Y. Egozy, S. Weiss, T-jump apparatus with microwave heating, *J. Phys. E. Sci. Inst.* 9 (1976) 366–367.
- [12] D. Stueriga, K. Gonon, M. Lallemand, Microwave heating as a new way to induce selectivity between competitive reactions. application to isomeric ratio control in sulfonation of naphthalene, *Tetrahedron* 49 (28) (1993) 6229–6234, [https://doi.org/10.1016/S0040-4020\(01\)87961-8](https://doi.org/10.1016/S0040-4020(01)87961-8), URL <<https://www.sciencedirect.com/science/article/pii/S0040402001879618>>.
- [13] A. de la Hoz, A. Diaz-Ortiz, A. Moreno, Microwaves in organic synthesis. Thermal and non-thermal microwave effects, *Chem. Soc. Rev.* 34 (2005) 164–178, <https://doi.org/10.1039/b41438h>.
- [14] G.B. Dudley, R. Richert, A.E. Stigman, Chemical Science On the existence of and mechanism for microwave-specific reaction rate enhancement, *Chem. Sci.* 6 (2015) 2144–2152, <https://doi.org/10.1039/c4sc03372h>.
- [15] D. Dallinger, C.O. Kappe, Microwave-assisted synthesis in water as solvent, *Chem. Rev.* 107 (2007) 2563–2591, <https://doi.org/10.1021/CR0509410>, URL <<https://pubs.acs.org/doi/abs/10.1021/cr0509410>>.
- [16] S. Horikoshi, N. Serpone, Role of microwaves in heterogeneous catalytic systems, *Catal. Sci. Technol.* 4 (2014) 1197–1210, <https://doi.org/10.1039/c3cy00753g>.
- [17] V.P. Mehta, E.V. Van der Eycken, Microwave-assisted C-C bond forming cross-coupling reactions: an overview, *Chem. Soc. Rev.* 40 (10) (2011) 4925, <https://doi.org/10.1039/c1cs15094d>, URL <<http://xlink.rsc.org/?DOI=c1cs15094d>>.
- [18] C.O. Kappe, How to measure reaction temperature in microwave-heated transformations, *Chem. Soc. Rev.* 42 (12) (2013) 4977, <https://doi.org/10.1039/c3cs00010a>, URL <<http://xlink.rsc.org/?DOI=c3cs00010a>>.
- [19] M. Azarkh, E.J.J. Groenen, Temperature Determination by EPR at 275 GHz and the Detection of Temperature Jumps in Aqueous Samples, *J. Phys. Chem. B* 119 (42) (2015) 13416–13421, <https://doi.org/10.1021/acs.jpcc.5b08353>, URL <<http://pubs.acs.org/doi/10.1021/acs.jpcc.5b08353>>.
- [20] J.J. Eckburg, J.C. Chato, K.J. Liu, M.W. Grinstaff, H.M. Swartz, K.S. Suslick, F.P. Aueri, The measurement of temperature with electron paramagnetic resonance spectroscopy, *J. Biomech. Engin.* 118 (2) (1996) 193–200, <https://doi.org/10.1115/1.2795959>, URL <<http://biomechanical.asmedigitalcollection.asme.org/article.aspx?articleid=1400394>>.
- [21] S. Stoll, A. Schweiger, EasySpin, a Comprehensive Software Package for Spectral Simulation and Analysis in EPR, *J. Magn. Reson.* 178 (1) (2006) 42–55, <https://doi.org/10.1016/j.jmr.2005.08.013>.
- [22] L. Korson, W. Drost-Hansen, F.J. Millero, Viscosity of water at various temperatures, *J. Phys. Chem.* 73 (1) (1969) 34–39, <https://doi.org/10.1021/j100721a006>.
- [23] B. Hammouda, Temperature effect on the nanostructure of SDS micelles in water, *J. Res. NIST* 118 (2013) 151–167.
- [24] R. Wilson, D. Kivelson, ESR Linewidths in solution. IV. Experimental studies of anisotropic and spin-rotational effects in copper complexes, *J. Chem. Phys.* 44 (1966) 4445–4452.